Experimental method to quantify the efficiency of the first two operational stages of nanosecond dielectric barrier discharge plasma actuators

Correale, Giuseppe; Avallone, Francesco; Yu Starikovskiy, A.

Important note
To cite this publication, please use the final published version (if applicable).
Please check the document version above.

Experimental method to quantify the efficiency of the first two operational stages of nanosecond dielectric barrier discharge plasma actuators

G.Correale[1], F. Avallone[2], A.Yu. Starikovskiy[3]

Abstract

A method to quantify the efficiency of the first two operational stages of a nanosecond Dielectric Barrier Discharge (ns-DBD) plasma actuator is proposed. The method is based on the independent measurements of the energy of electrical pulses and the useful part of the energy which heats up the gas in the discharge region. Energy input is calculated via a back current shunt technique as the difference between the energy given and the energy reflected back. The ratio of the difference of the latter two quantities and the energy input gives the electrical efficiency (η_E) of a ns-DBD. The extent of the energy deposited is estimated via Schlieren visualizations and infrared thermography measurements. Then, the ideal power flux obtained if all the inputted energy was converted into heat is calculated. Transient surface temperature was measured via infrared thermography and used to solve a one-dimensional Inverse Heat Transfer Problem (IHTP) in a direction normal to the surface. It gives as output the actual power flux. The estimated ratio between the two power fluxes represents a quantification of the mechanical fluid efficiency (η_{FM}) of a ns-DBD plasma actuator. Results show an inverse proportionality between η_E, and η_{FM}, and the thickness of the barrier. The efficiency of the first two operational stages of a ns-DBD is further defined as $\eta = \eta_E \cdot \eta_{FM}$.

---

1 PostDoc Researcher, Delft University of Technology, The Netherlands. email: g.correale@tudelft.nl

2 PostDoc Researcher, Delft University of Technology, The Netherlands.

3 Senior researcher, Princeton University, New Jersey, USA.

Introduction

Unsteady flow control techniques [1] that use periodic excitations to manipulate flow stability [2,3] have the potential to overcome any other active flow control technique in terms of efficiency [4] because of the relatively low amount of energy they use. DBD (Dielectric Barrier Discharge) plasma actuators belong to this category.

Theoretical, experimental and numerical investigations have proven DBD plasma actuators [5,6] to be an effective means of active, unsteady flow control. There exist two kinds of DBD plasma actuators, namely AC-DBD and ns-DBD; the former driven by Alternating Current (AC), the latter by high voltage nanosecond (ns) pulses. These actuators are very similar in their layouts, materials and constructive methodologies; however, their flow control mechanisms, based on manipulation of the natural stability of the controlled flow [7,8] are very different. The AC variant is capable of inducing a volumetric force on the controlled flow [9,10], while the nanosecond variant induces an especially strong thermal effect on the portion of gas-flow within the discharge volume, thus producing a density/viscosity gradient [11].

These devices can be also used for applications other than flow control. Recently, the authors have applied ns-DBDs to develop a de-icing system in still air [40].

Before using these devices in industrial applications, it is important to quantify their efficiency. The first attempt to provide a guideline for the evaluation of the efficiency of AC-DBD is reported by Roth and Dai [12], work later expanded by Kriegseis et al. [13,14,15].

Following their works, a DBD actuator passes through three stages of operation, each one having a contribution to the overall efficiency and each one suffering from energy losses. The first stage is related to the electrical discharge (η_E), the second to the physical mechanism of flow control (different for different kinds of plasma actuators, η_{FM}) and the third one is related to the flow control task to be achieved (η'_S) [13,14].

According to Kriegseis et al. [13,14,15] the efficiency of the first operational stage is defined as the ratio between the discharge power P_A and the electrical input power P_{input}; it is a non-dimensional coefficient that ranges between 0 and 1 [15]. The second stage is defined as the ratio between the fluid mechanic (output) power P_{FM} and the discharge power P_A. However, due to the fact that the mechanism of flow control for AC-DBDs is based on the input of a volumetric force, very often a method that is used to characterize their fluid mechanic output is to measure the induced thrust force. This does not allow one to determine power, given the absence of velocity information. Therefore, the efficiency of the second operational stage is often substituted by a dimensional coefficient called effectiveness that ranges between 0 and 1 [16,17,18]. This method to quantify efficiency cannot be applied for the ns-DBDs, since their control mechanism is based on a thermal effect [19,20]. The goal of this work is to present a method to quantify η_{FM} for ns-DBDs. The efficiency of the third operational stage of an AC-DBD is a non-dimensional coefficient larger than 1 [15], since it is the ratio between the energy gained by applying flow control and the energy consumed to actuate the flow. Therefore, it is related to the flow control task to be achieved and its calculation is straightforward according to the literature [13,14,15]. For this reason, and because the estimation of the first two stages of efficiency is necessary in other cases (i.e. de/anti-icing), the third stage is not further considered in this manuscript.

Regarding the first and second stage of efficiency, three sources of energy loss are recognised [12]: the first source of energy loss is due to an impedance mismatch between the actuator and the electrical feeding system (related to η_E); the second is due to the heating of the dielectric barrier (related to η_{FM} mainly affecting the ns-DBD variant); the third is due to the rate of the ionization of particles and the energy required to sustain plasma at atmospheric pressure (related to η_{FM} mainly affecting the AC-DBD variant). For ns-DBDs quantification of the energy losses within the barrier is of vital importance in order to define the efficiency of energy deposition within the discharge volume.

In order to quantify the second stage of efficiency of a ns-DBD plasma actuator, it is necessary to quantify the first and the second contribution to the energy losses [12]. In this respect, internal losses

are not just dependent on geometric characteristics [21,22] but also on the thermal properties of the dielectric material used as a barrier [23]. Therefore, during discharge some energy flows throughout the barrier and diffused or stored within the dielectric barrier. This happens on the time scale of the discharge (i.e. nanosecond, [21]) and, together with the energy reflected back into the feeding system due to impedance mismatches, it represents the first part of the energy losses. On the time scale of residual heat increase within the discharge volume (i.e. milliseconds, [8,24]), heat generated by the discharge is conducted through the barrier and diffused internally. These are the main contributors to the energy losses of a ns-DBD.

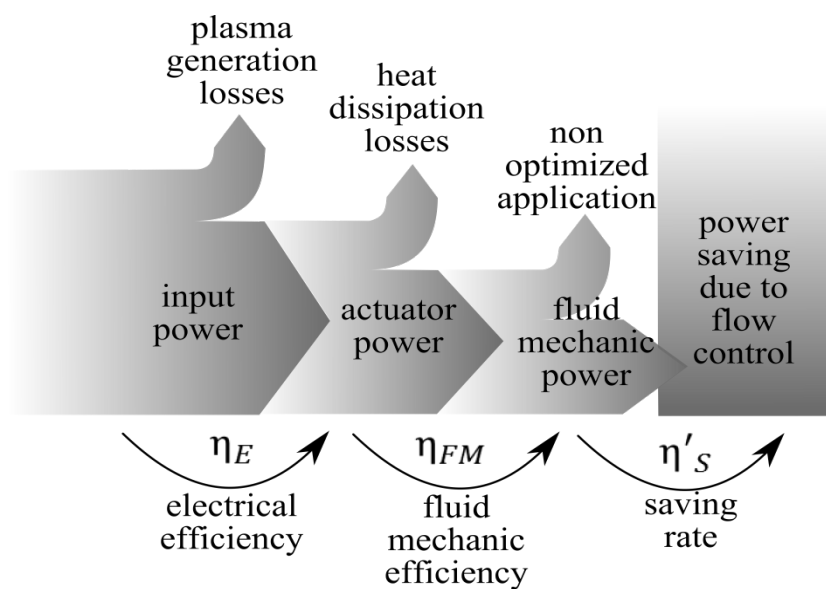In figure 1 a sketch of the energy budget is given.

Figure 1. Sketch of the energy budget for a ns-DBD plasma actuator adapted from [15].

In this paper, an experimental approach is provided to measure η_E via a back-current shunt technique [8,23], while quantification of η_{FM} is carried out via Schlieren and infrared thermography acquisitions that are used to determine the physical extent of the discharge and to solve an Inverse Heat Transfer Problem (IHTP) [25]. The difference between the power flux input estimated by solving the IHTP and the ideal power flux input obtained if all the energy input contributed to the thermal effect of a ns-DBD approximates the net energy losses. The ratio between the latter two quantities gives, with good

approximation, the efficiency of η_{FM} for ns-DBD plasma actuators. Eventually, a characterization of the thickness of the dielectric barrier is performed to test the proposed method.

Experimental setup

Plasma actuator

A nanosecond dielectric barrier discharge plasma actuator is constructed using two electrodes made out of adhesive copper tape and separated by a dielectric barrier. The actuator is flush-mounted on an upside-down flat plate (in order to minimize the effects of natural convection) and placed in a still air environment. Electrodes are placed right beside each other, i.e. there is zero horizontal distance between them. The embedded electrode is encapsulated in an extra layer of dielectric material to avoid unwanted discharges. A sketch of the plasma actuator layout is given in figure 2, together, with the used reference system.
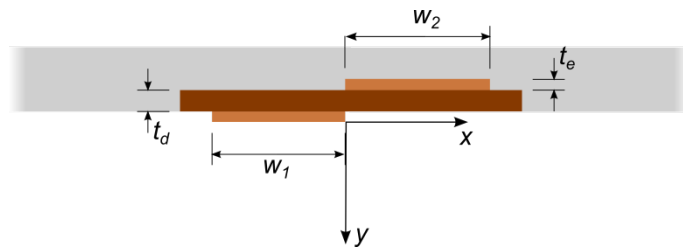

Figure 2. Sketch of ns-DBD plasma actuator layout and Cartesian coordinate system.

Due to the limitations on the depth of heat penetration Kapton tape, which is used in most of the cases in the literature [5,6], is not suitable for this study (see the section Heat Transfer Data Reduction for more details). The material selected instead of Kapton for the barrier is Lexan® because of its well-known thermal and electrical properties. Three thicknesses are investigated: 0.5, 0.75 and 1 mm. The length of the copper electrodes is 15 cm with a width of 6.3 mm. The thickness of the self-adhesive electrodes is 60 μm with an additional 29 μm of silicon-based adhesive between the electrode and the dielectric layer. An overview of the characteristics of the tested actuators is listed in table 1.

Table 1. Tested ns-DBD plasma actuator characteristics.

Symbols	Description	Value
W_1	Exposed electrode [mm]	6.3

W_2	Covered electrode [mm]	6.3
t_d	Dielectric thickness [mm]	0.5/0.75/1
t_e	Electrode thickness [mm]	<0.1
Sp	Actuator length [mm]	150
V_p	Pulse voltage [kV]	10

The actuators are operated via an Arbitrary Function Generator (AFG) and powered by a FID solid-state power supply capable of delivering a pulsed high voltage signal of about 23 ns, with a rising time of 3 ns (from 10 % to 90 % of the maximum voltage). The maximum voltage and the maximum frequency are 10 kV and 10 kHz respectively (same power generator was used in [19]). The investigated energy input consists of a burst of 50 pulses discharged at maximum voltage and frequency.

Back-current shunt

Power measurements are performed via the back-current shunt technique [26,27,28] in order to calculate energy associated with a single pulse. This is an indirect technique relying on the measure of incident and the reflected current running through the actuator circuit.

A shunt monitor resistor is built using 16 resistors, of 3.2 Ω each, placed in parallel, resulting in an overall shunt resistance of 0.2 Ω. In figure 3 an electrical scheme of the set-up is given for reference.
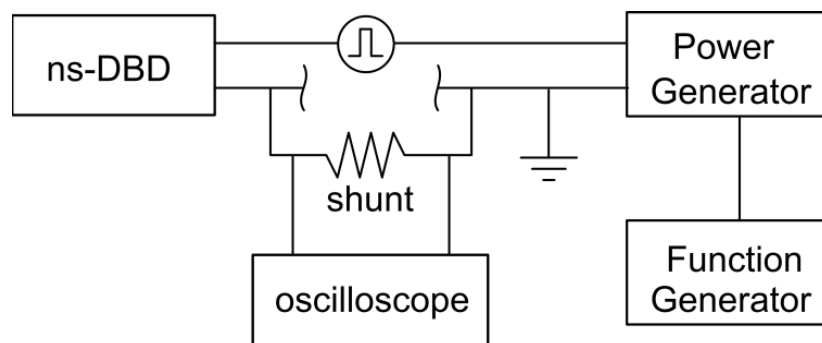

Figure 3. Electrical setup of back-current shunt technique.

The shunt resistor is placed in the middle of the ground electrode of a 20m long high voltage coaxial cable (type RG-217). This high voltage cable is used to deliver the high voltage nanosecond pulse from

the power generator to the tested plasma actuator. The shunt resistor is calibrated by applying a known signal of 5 V from an AFG (Tektronics AFG3252) and measuring the voltage across the shunt directly using a digital oscilloscope with a sampling frequency of 1 GHz set at an impedance so as to match the impedance of the high voltage cable, i.e. 50 Ω. For the actual measurements, a 20 dB signal attenuator is used in order to protect the oscilloscope from voltage overload. The attenuation constant of the shunt resistor K_{sh} is theoretically calculated to be 250 using:

$$K_{sh} = \frac{Z}{R_{sh}}$$

(0)

where Z is the impedance of the high voltage cable and R_{sh} is the total resistance of the shunt; 50 and 0.2 Ω, respectively. The calibration process yielded a K_{sh} value of 253.97, which is very close to the value calculated.

Measurements of pulse energy are performed by measuring the voltage across the shunt resistor directly with the oscilloscope. The application of a high voltage nanosecond pulse from the power generator can be observed as a scaled voltage pulse over the shunt, measured by the oscilloscope.

Schlieren imaging

Time-resolved Schlieren measurements are carried out in order to visualize and quantify the size of the thermalized area in the discharge-wise direction resulting from ns-DBD actuation. A 12-bit CCD 4 Megapixel (2016 x 2016 pixel) La Vision Imager pro HS 4M camera is used. The camera allowed measurements at 1 kHz full frame, with an exposure time of 2 μs. Synchronization between camera and actuator is achieved using an AFG. A beamer Arc Lamp (Solarc, Lighting Technology) is used as light source of about 50 W. The Schlieren setup is arranged in Z configuration. Magnification is about 0.2, while the FOV is approximately 11 x 11 cm^2, i.e. about 0.055mm/pixel. A spatial filter is configured to provide a density gradient along the vertical axis. A sketch of the arrangement for the Schlieren experiments is shown in figure 4.
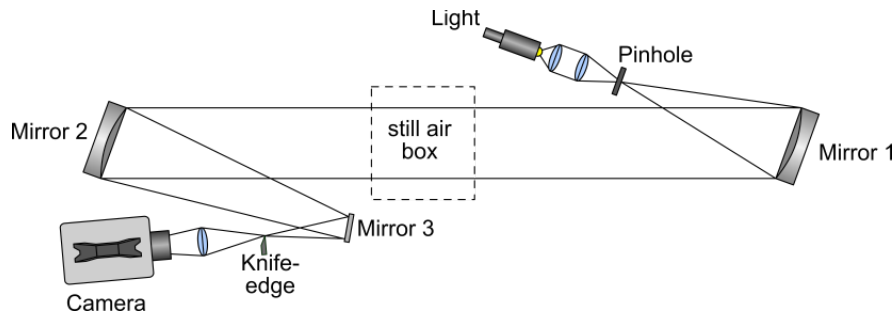
Figure 4. Schematics of Schlieren experimental set-up arrangement.

Infrared thermography

Infrared thermography [29] is used to map the transient temperature distribution of the dielectric barrier surface induced by a nanosecond high voltage pulsed discharge. A sketch of the setup arrangement is presented in figure 5. The measurements are performed using a CEDIP Titanium 530L IR camera. It has a mercury cadmium telluride (MCT) quantum detector array of 320 x 256 pixels and a spectral response of 7.7–9.3μm. The sensor is cooled to 77K by the Stirling cycle and has a NETD (Noise Equivalent Temperature Difference) of 25mK. The integration time of the camera is set to 400 μs, while the acquisition frame rate is 200 Hz. A germanium lens with a 25mm focal length set at $f^{\#}=2$ is employed to obtain a spatial resolution of approximately 2 pixels $\cdot$ mm^{-1} (or 0.5 mm pixel^{-1}), with a magnification of 0.06. The camera is located on a traverse system and the ns-DBD actuator is imaged through a parabolic mirror in order to increase image magnification. The IR acquisition system is calibrated using a black body built in-house [30] and the mirror is kept installed during the calibration process to take into account IR emission losses [31]. The viewing angle with respect to the model surface is kept smaller than 50 degrees such that the emissivity of Lexan® can be regarded as constant and independent of the viewing angle [29]. The transient temperature acquisition started 400μs after the end of the discharge in order to avoid electromagnetic interference and recorded for 100ms.
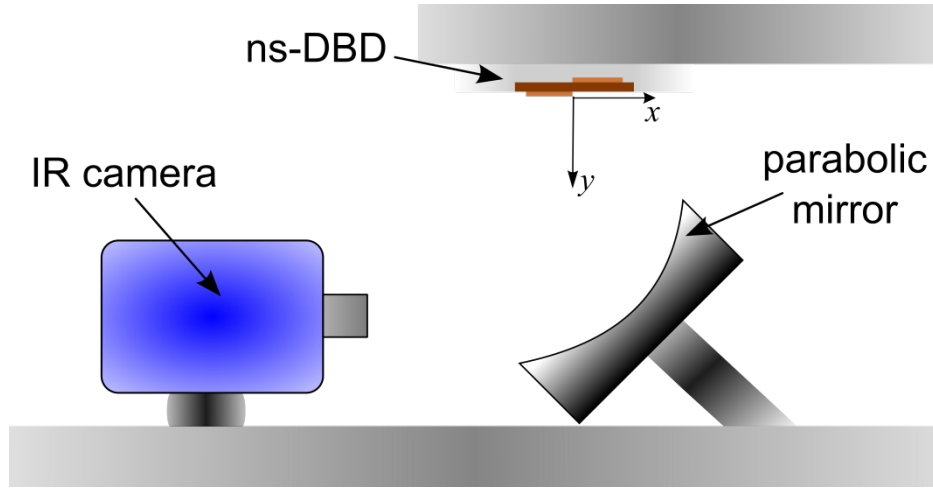
Figure 5. Sketch of IR thermography set-up. Actuator dimensions are exaggerated for clarity.

Inverse Heat Transfer Data Reduction

The wall heat flux distribution is computed from the surface temperature signal by solving a one-dimensional IHTP based on the semi-infinite slab model coupled with a least squares approach [25,32]. Starting from the temperature dynamics of the barrier, the heat flux (q) is evaluated by minimizing the difference between the computed temperature drop (eq. 2), and the measured experimental one. The optimization is performed by means of the Trust Region Reflective algorithm. The numerical rise in temperature is computed by solving the heat equation inside the body with the boundary conditions as indicated below:

$$k \nabla^2(T) = \rho c_p \frac{\partial T}{\partial t}$$
$$T(x_0, y_0, z, 0) = T_{wi}$$
$$k \left. \frac{\partial T(x_0, y_0, z, t)}{\partial n} \right|_S = q(t) \wedge T(x_0, y_0, z \in F, t) = T_F(t)$$

(2)

where (x_0, y_0) are the pixel coordinates in which the temperature is measured, S is the barrier surface exposed to the discharge while F is the opposite surface at a constant temperature. Here, k, ρ and c_p are the thermal conductivity, the density, and the specific heat of the barrier material (see table 2), T_{wi} is the initial temperature, and q is the heat flux due to the discharge.

Symbols	Description	Value
c_p	Specific heat [J/kg K]	1210
K	Thermal conductivity [W/m K]	0.2
P	Density [kg/m³]	1.245
V_ρ	Volumetric resistivity[Ωm]	10^{15}
ε_r	Relative permittivity[-]	3

The heat flux is modelled as follows:

$$q=q_o \, t \leq \frac{n_{pulses}}{f}$$
$$q=0 \, t > \frac{n_{pulses}}{f}$$

(3)

where f is the discharge frequency and n_{pulses} is the number of pulses within a burst. In the current investigation, the discharge is modelled as a continuous and time-constant heat source (q_o) acting over the given discharge time n_{pulses} /f. At the end of the discharge the heat flux is set equal to zero and the temperature of the surface exposed to the discharge drops due to heat conduction within the material.

The heat flux might be modeled resembling closely the actual physics, i.e. as a time series of pulses with time constant or variable intensity. The time length of fast gas heating induced by each pulse might be of the order of hundreds of nanoseconds as in literature [24,41]. However, the assumption of constant heat flux made in eq. 3 is still valid to show the applicability of the IHTP to measure the efficiency of the first two operation stages of a ns-DBD plasma actuator.

In the current analysis, natural convection is neglected because of gas stratification induced by the upside-down configuration.

The initial temperature distribution, T_{wi} , is known from the measurements and it is considered to be constant over the entire domain. A known temperature T_F is used as boundary condition at the wall not exposed to the discharge (F). The wall F is considered isothermal so that

$$T \, \lambdabar \, (x_0, y_0, z \in F, t) = T_{wi}$$. The assumption can be considered valid if the penetration depth (

$d_p = 4\sqrt{\alpha t}$ where $\alpha = 1.4 \, x \, 10^{-7} m^2 s^{-1}$ is the material thermal diffusivity and t is the time-scale of the energy [33]) is smaller than the thickness of the material. It was verified that the assumption was valid for the tested actuators. Furthermore, such limitations on the penetration depth imposed the use of a material other than Kapton. According to preliminary calculations, in order to have the penetration depth be smaller than the thickness of the barrier, a thicker layer of Kapton tape had to be used. However, each layer of Kapton tape is coupled with a layer of silicone-based glue, whose properties are unknown. This would have introduced a high uncertainty in modelling the barrier. Therefore, in order to use a barrier with well-known thermal and electrical properties and low impurity, Lexan was employed for this study instead of Kapton tape.

The heat transfer problem is solved using parabolic partial differential equations. The time integration is performed using a backward approach. The spatial discretization is made evaluating the convergence of the solution of the heat equation.

An example of fitting between the experimental data and the solution of the heat equation is reported in figure 6. In this figure the calculated and measured temperature evolutions refers to the spanwise average over the length of the actuator in the z-axis (see figure 2).
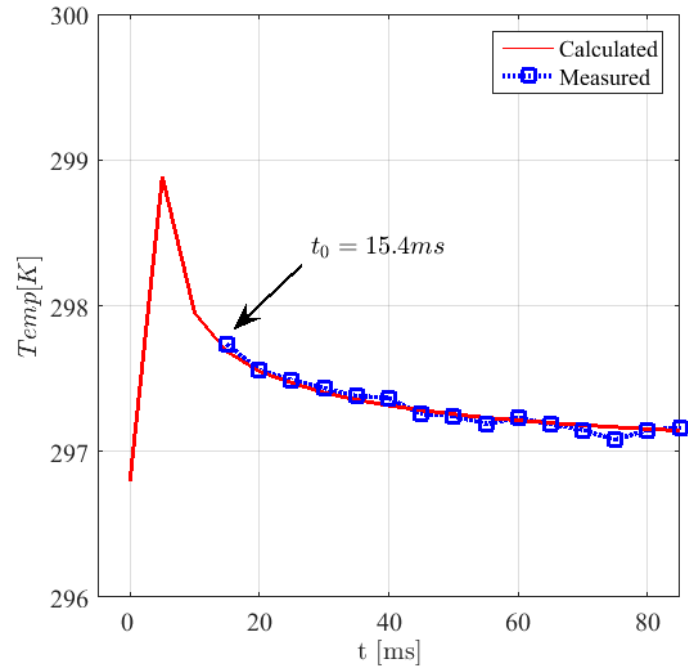
Figure 6. Example of best fit between the experimental data and the temperature history obtained by solving the IHTP (equation 1). In the figure the black arrow indicates the initial instant time t_0 of measurements.

Results

Electrical efficiency

Energy input is calculated from the driving voltage signal measured via the back-current shunt technique. In figure 7 a typical discharged pulse (V_{app}) as measured across the shunt, is presented.
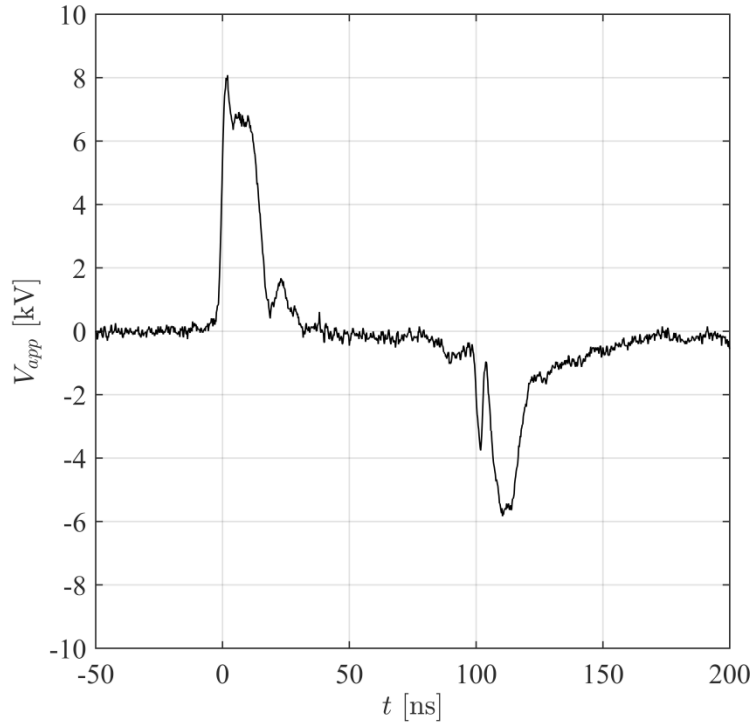
Figure 7. V_{app} is a typical high voltage driving signal calculated through the back current shunt measurements as function of time (t) in nanoseconds.

During the first 200 ns, the voltage signal presents two peaks. The first peak represents the total electrical energy input given by the power generator (E_{in}) while the second peak represents the energy reflected back within the system (E_{ref}). Given the time scale of the discharge, according to transmission line theory [34], energy contained in each single nanosecond pulse can be calculated as:

$$P_{¿}\,dt = ¿\int V_{¿}\,I_{¿}\,dt = \int \frac{V_{¿}^2}{Z}\,dt$$
$$E_{¿} = \int ¿$$

(4)

where V_{in} and I_{in} are the voltage and the current input, respectively, and Z is the impedance of the high voltage cable. The pulse current can be calculated as $I = V/Z$ [34]. The reflected pulse current can be estimated using the same approach. Note that the discharge energy can be calculated as a difference between the energy of incident and the reflected pulses without measuring the pulse currents [34]:

$$\Delta E = E_i - E_{ref} = \int \frac{V_i^2}{Z} dt - \int \frac{V_{ref}^2}{Z} dt \qquad (5)$$

Thus

$$E_{pp} = E_i - E_{ref} \qquad (6)$$

where E_{pp} is the net electrical energy per pulse deposited within the discharge volume and lost

internally by the plasma actuator itself.

The calculated values of the averaged net energy input per pulse and per burst (obtained by

multiplying $E_{pp} \cdot n_{pulses}$), for each investigated barrier thickness, are given in table 3.

Table 3. Averaged energy input per pulse and per burst, for each thickness investigated.

Thickness	0.5	0.75	1	Units [mm]
Averaged E_{pp}	7.2×10^{-3}	6.1×10^{-3}	5.4×10^{-3}	[J]
E_{pp} per burst	3.59×10^{-1}	3.07×10^{-1}	2.68×10^{-1}	[J]

The power drained from a DBD actuator is dependent on the load of the system itself [12,15,22]

which is composed of two parts, one purely passive that depends on the actuator construction

characteristics (geometry, material, etc.) and the other is discharge dependent, meaning it is a

function of electrical characteristics. Electrical efficiency η_E is therefore the ratio between the energy

input and the energy drained, defined in equation 7:

$$\eta_E = \frac{E_i - E_{ref}}{E_i} \qquad (7)$$

Results calculated for the investigated case are reported in table 4.

Table 4. Electrical efficiency η_E calculated for the investigated cases.

thickness	0.5	0.75	1	Units

				[mm]
η_E	0.51	0.44	0.39	N/A

The electrical efficiency is inversely proportional to the thickness of the barrier, i.e. the thinner the barrier the higher η_E. Such behavior is due to the fact that a thinner barrier corresponds to a larger electrical field between the electrodes, which induces a stronger discharge [23, 38,39]. This result is in line with the literature [21].

The impedance of the SDBD varies from infinity (during the discharge ignition delay time) to some steady-state value Rd. This Rd depends on the charge transfer dynamics in the discharge gap. Typically, we charge the capacitor formed by a conductive plasma layer, a dielectric layer, and a covered electrode until it reaches the potential of a high-voltage electrode. The capacitance is inversely proportional to the thickness of the dielectric layer and increases when the ionization wave propagates from the edge of the high-voltage electrode. The velocity of the propagation of the ionization wave dramatically increases with the electric field value. The electric field in the SDBD geometry increases when the dielectric layer thickness decreases. Thus, the decrease of the dielectric layer thickness leads to an increase in SDBD linear capacitance and to an increase in the rate of plasma layer propagation. This means that the smaller dielectric thickness decreases the discharge gap impedance and reduces the reflection of the high-voltage pulse from the discharge.

Thus, it is expected that increasing the thickness of the barrier the efficiency decreases (see table 4).

Fluid mechanic efficiency

In order to convert the calculated net energy input into power flux, the area of the heated region must be estimated. The area is calculated by multiplying the span length (*Sp*) of the tested actuators (table 1) and the size of the heated region in the *x*-direction, referred to as L_e. Both Schlieren and infrared thermography techniques are employed to measure L_e.

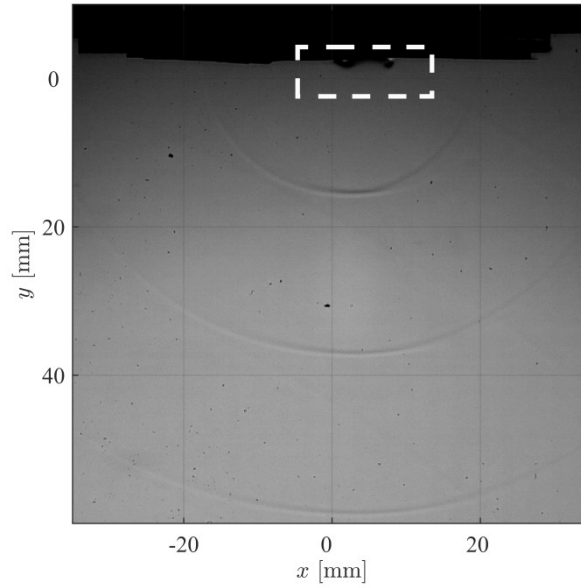In figure 8 an example of a Schlieren visualization is demonstrated.

Figure 8. Example of a Schlieren visualization of the discharge volume. The white dashed rectangle represents the region where post processing was carried out. The magnified image of this area is shown in figure 9.

The image represents the side view (parallel to the *x-y* plane, see figure 2) of the tested ns-DBD plasma actuator with a 0.5 mm barrier, 5 ms after the beginning of the discharge of a 50 pulse burst. The air affected by the heat transfer changes its density thus revealing the size of the heated volume [8,23]. It is possible to appreciate all the typical features of a nanosecond pulsed high voltage discharge, i.e. cylindrical and planar shockwaves and residual heat, as reported in literature [19,20,35]. A white dashed rectangle highlights the region of interest. This region of interest is reported raw (top row) and processed (bottom row) in figure 9 for all the investigated cases.
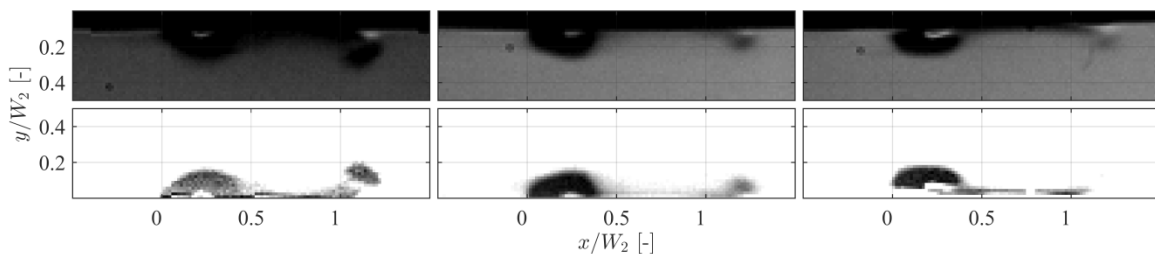

Figure 9. Discharge volume 5 ms after the start of discharge, induced by a burst of 50 pulses at 10 kHz. Raw (top row) and processed (bottom raw) data. From left to right, results of the 0.5, 0.75 and 1 mm dielectric barrier thickness respectively. The length of the covered electrode (W_2, see table 1) is used to make the figure non-dimensional.

The images are processed with a method to qualitatively characterize the energy input [8,23,36,38] making the figure more easily readable. Axes are made non-dimensional with respect to the width of the covered electrode W_2 (see table 1) so to keep constant the aspect ratio of the images. The only information of interest in this case is the discharge-wise size of the heated volume (L_e), which is obtained by a spatial calibration. One can measure L_e as a simple count of the number of pixels involved in the gas heating in the x-direction. Then, this length in pixels is converted into millimeters via a spatial calibration of the images.

It is clear from figure 9 that in all the cases the volume affected by a density change extends in the x-direction so as to have L_e be larger than the covered electrode W_2. This phenomenon is attributed to the small body force produced by the ns-DBD [11,37]. Hot air transported in that region contributes to the wall heat transfer.

In figure 10, temperature (10a and 10b) and heat flux (10c and 10d) profiles obtained by solving the IHTP are reported.
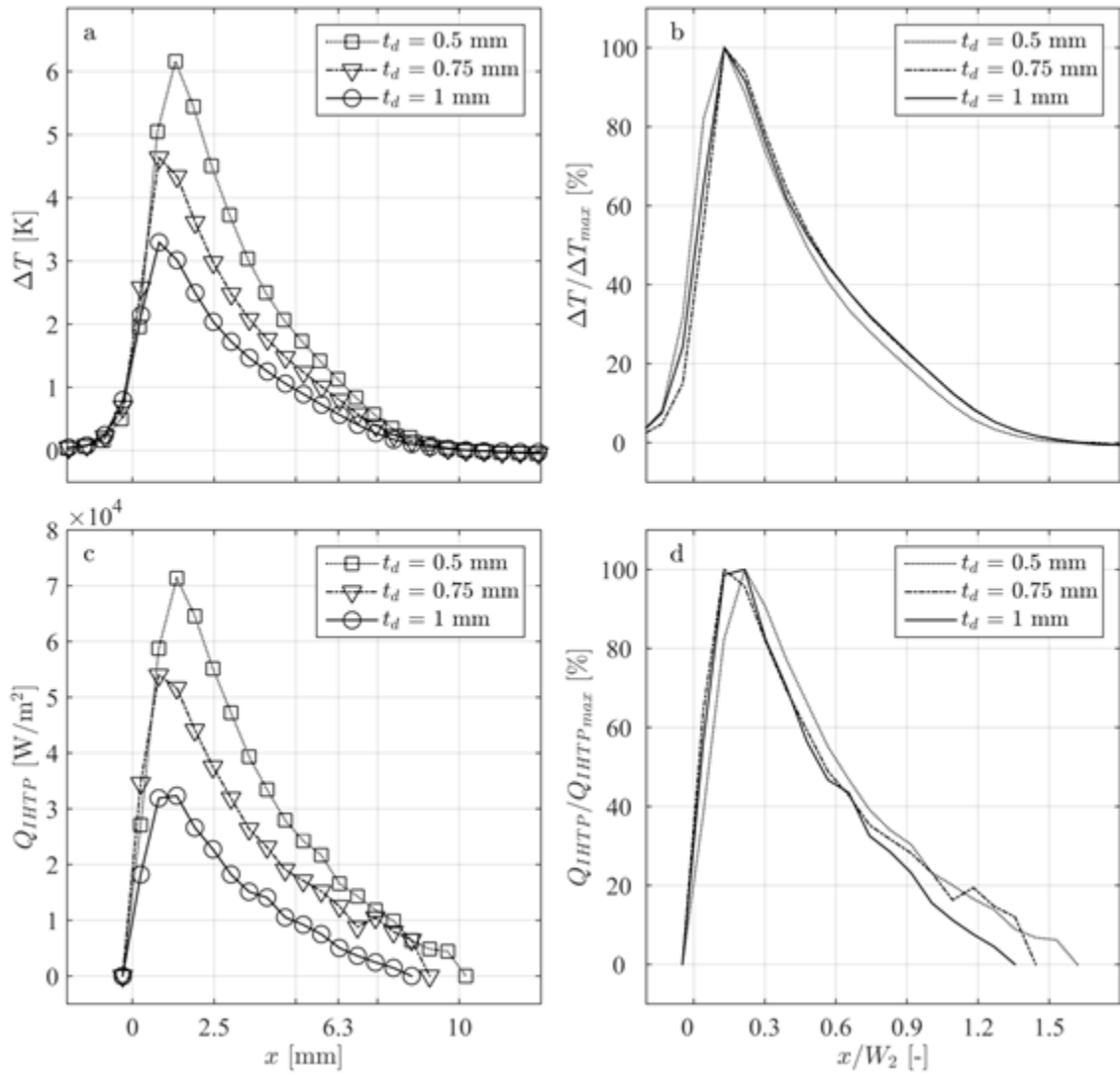
Figure 10. Top row. Spanwise average of the temperature map measured at $t_0 = 15.4$ ms after the beginning of the discharge of a burst of 50 pulses at 10 kHz, dimensional (a) and non-dimensional (b). Bottom row. Power flux calculated from IR thermography measurements solving an IHTP in dimensional form (c) and non-dimensional (d).

The subplots 10b and 10d are made non-dimensional with respect to the local maximum and the length of the covered electrode W_2 (see table 1). It is also noted that temperature measurements (figure 10a and 10b) show that L_e is larger than the length of the covered electrode, indicating that the heated volume of air pushed by the induced body force contributes to the heating of the barrier surface. In table 5 the dimensions of L_e are reported, as measured with both Schlieren and infrared thermography.

Table 5. Estimated energy deposition length Le in the x-direction.

Units

thickness	0.5	0.75	1	[mm]
L_e via Schlieren	8.19	7.875	7.56	[mm]
L_e via Thermography	10.1	9.12	8.51	[mm]

It is noted that the values obtained using thermography are larger. This phenomenon is attributed to thermal diffusion and internal conduction in the x-direction. Moreover, the difference between the lengths measured using the two different methods decreases when the thickness of the dielectric layer increases. This is due to both a reduced body force that induces a smaller diffusion of the heated volume and a reduced thermal transfer rate. The reduction of the thermal transfer is due to the internal conduction in the x-direction because of the temperature increase on the lower surface.

Due to the smaller amount of uncertainties in the Schlieren measurement, in the following, L_e measured via Schlieren is the reference length used to calculate Q_E, i.e. the ideal power flux obtained if all the energy input was deposited into the discharge volume and converted into heat. If all the electrical energy input (see table 3) contributes to the heating of the discharge volume with an energy deposition efficiency of 100 %, the generated power flux Q_E can be calculated as:

$$Q_E = \frac{\eta_E E_{in} n_{pulses}}{\Delta t \, L_e \, Sp}$$

(8)

where η_E is the electrical efficiency as defined in equation 7, E_{in} is the energy input (averaged here over 21 samples per each tested case), n_{pulses} is the number of pulses, Δt is the period of the burst, Sp is the length of the actuator span (see table 1) and L_e is the extension of the heated volume in the x-direction as measured via Schlieren (see table 5).

In figure 10c and 10d the heat flux calculated with the IHTP are reported. In the following, the span wise mean heat flux computed solving the IHTP described above ($Q_{IHTPmean}$) for each thickness is used to calculate η_{FM}. Both Q_E and $Q_{IHTPmean}$ are reported in table 6.

Table 6. Mean heat flux obtained via IHTP ($Q_{IHTPmean}$) and the ideal one estimated from experiments (Q_E).

				Units
thickness	0.5	0.75	1	[mm]
$Q_{IHTP_{mean}}$	2.83 x 10^4	2.32 x 10^4	1.43 x 10^4	[W/m^2]
Q_E	5.84 x 10^4	5.4 x 10^4	5.15 x 10^4	[W/m^2]

From table 6 it can be observed that both Q_E and $Q_{IHTPmean}$ decrease as the thickness of the barrier increases. This is due to the fact that the energy deposition is dependent on the characteristics of the barrier, i.e. the thicker the barrier, the smaller the amount of energy deposited into the discharge volume [23,38]. The ratio between the two power fluxes presented in table 6 is considered to be the efficiency of the second stage of operation of the tested ns-DBD plasma actuator η_{FM}, as defined in equation 9:

$$\eta_{FM} = \frac{Q_{IHTPmean}}{Q_E}$$ (9)

Results are reported in table 7 for the all the cases investigated.

Table 7.Fluid mechanic efficiency η_{FM} of the tested ns-DBDs.

				Units
thickness	0.5	0.75	1	[mm]
η_{FM}	0.49	0.43	0.28	N/A

The difference between the energy given as an input by each pulse and the energy reflected back into the cable represents the energy given as an input to the ns-DBD actuator. Q_E is the maximum heat flux that might be generated if all the input energy is transformed into heat. On the other hand, $Q_{IHTPmean}$ is the heat flux measured by solving the IHTP. The difference between the two contributions (Q_E - $Q_{IHTPmean}$) represents the energy loss, i.e. the fraction of energy that is not converted into heat and does not contribute to the heating of the surface of the dielectric barrier.

With the values reported in tables 4 and 7 it is possible to find the efficiency of the tested ns-DBD plasma actuators, defined as:

$$\eta = \eta_E \eta_{FM}$$ (10)

Results are reported in table 8.

Table 8. Fluid mechanic efficiency η of the tested ns-DBDs.

				Units
thickness	0.5	0.75	1	[mm]
η	0.25	0.19	0.11	N/A

η gives the fraction of consumed energy that actively contributed to the actuation effect.

Table 8 shows that, as expected, the efficiency of the first and the second operational stages of a ns-DBD is reduced by increasing the barrier thickness. This is due to the fact that increasing the thickness of the barrier, increases the energy loss. In particular, the distance between the two electrodes increases when the barrier thickness increases, thus a weaker electrical field is formed and consequently less energy is discharged for a given energy input. Moreover, increasing the thickness of the barrier results in an increase of the capacitance of the actuator itself [21]. This results in an increase of the impedance mismatch between the actuator and the feeding system, increasing the energy losses, and reducing efficiency. From a thermodynamic point of view, an increase in thickness will also result in an increase in thermal energy loss due to thermal diffusion within the material and tangential conduction (the second factor might be taken into account solving a two dimensional IHTP [32]). Therefore, a thicker barrier corresponds to a lower efficiency. An efficiency equal to zero is reached, then, when the barrier thickness is so large that the electrical discharge does not happen. During the experiment, it was observed that the discharge was almost absent for a barrier thickness equal to 1.25 mm, thus suggesting that in this case the efficiency tends to zero. Extrapolation of the data presented in table 8 shows that η equal to zero is reached for a barrier thickness equal to 1.27 mm, thus suggesting the validity of the proposed methodology. This last observation suggests that the assumption made on the heat flux of eq.3 is not far from reality.

Conclusion

In this paper an experimental method is presented to quantify the efficiency of a ns-DBD plasma actuator. The overall efficiency was sub divided into two parts. The first part is an electrical efficiency of the discharge, η_E. It characterizes the efficiency of the energy delivery from pulse generator to gas discharge. The second part, η_{FM}, represents the fraction of discharged energy that actively contributes to the thermal effect induced by a ns-DBD plasma actuator. The rest of the energy is reflected from the discharge gap back to the generator or is spent on unwanted surface heating.

The proposed approach consists of three steps:

1) The net electrical energy input is first measured via a back-current shunt technique. Then the net energy input is converted into power flux based on the period of the discharge and the dimension of the heated region measured via Schlieren. It represents the hypothetical power flux generated if all that discharged energy was converted into heat.

2) Then, measurements of the barrier surface temperature are carried out by means of infrared thermography. Transient temperature data is used to solve a 1D IHTP assuming that both tangential conduction and natural convection are negligible. Moreover, the assumption of a time constant heat flux during the discharge time is made such that the calculations are considered to be conservative.

3) The difference in powers measured at steps one and two gives the quantification of the total energy losses, while their ratio gives the fluid mechanic efficiency, η_{FM}.

A characterization of the dielectric barrier thickness is performed as well, in order to evaluate the performances of the method. There was found to be an inverse proportionality between the thickness of the dielectric barrier and the energy deposition (the thicker the barrier, the lower the η). Such expected results give confidence in the capability of the proposed method to measure efficiency. Thus the practical efficiency of a ns-DBD is limited by the electrical properties of the dielectric layer. The higher the critical electric field for breakdown and the higher the dielectric permittivity of the dielectric layer, the better the efficiency of the actuator.

Extending the measurements to a much wider range of barrier parameters or improving the modeling of the heat flux as given in eq.3 would also give the chance to improve the accuracy of the estimated efficiency and verify the obtained trends. The definition of η paves the way for characterization studies aiming at bridging the gap between this technology and its industrial application.

Acknowledgments

Bibliography

1. Gad-el-Hak, M. 2000

   Flow Control: Passive, Active, and Reactive Flow Management

   Cambridge University Press, C. U. (Ed.), Cambridge (UK).

2. Seifert, A.; Darabi, A. & Wygnanski, I. 1996

   Delay of airfoil stall by periodic excitation

   J Aircraft, 33 (4), 691-698

3. Greenblatt, D. & Wygnanski, I. J. 2000

   The control of flow separation by periodic excitation

   Prog Aerosp Sci, 36 (7), 487 - 545

4. Cattafesta, L. & Sheplak, M. 2011

   Actuators for active flow control

   Annu Rev Fluid Mech, 43, 247-272

5. Moreau, E. 2007

   Airflow control by non-thermal plasma actuators

   J Phys D Appl Phys, 40 (3), 605-636

6. Corke, T. C.; Post, M. L. & Orlov, D. M. 2009

   Single dielectric barrier discharge plasma enhanced aerodynamics: Physics, modeling and

   applications

   Exp Fluids, 46 (1), 1-26

7. Grundmann, S. & Tropea, C. 2008

   Active cancellation of artificially introduced Tollmien-Schlichting waves using plasma

   actuators

   Exp Fluids, 44 (5), 795-806

8. Correale, G.; Michelis, T.; Ragni, D.; Kotsonis, M. & Scarano, F. 2014

    Nanosecond-pulsed plasma actuation in quiescent air and laminar boundary layer

    J Phys D Appl Phys, 47 (10), 105201

9. Enloe, C.; McLaughlin, T.; VanDyken, R.; Kachner, K.; Jumper, E. & Corke, T. 2004

    Mechanisms and Responses of a Single Dielectric Barrier Plasma Actuator: Plasma

    Morphology

    AIAA J, 42 (3), 589-594

10. Enloe, C.; McLaughlin, T.; VanDyken, R.; Kachner, K.; Jumper, E.; Corke, T.; Post, M. & Haddad,

    O. 2004

    Mechanisms and Responses of a Single Dielectric Barrier Plasma Actuator: Geometric Effects

    AIAA J, 42 (3), 595-604

11. Correale, G.; Winkel, R. & Kotsonis, M. 2016

    Induced density gradient by ns-DBD plasma actuator on flat plate boundary layer

    AIAA Journal (in press)

12. Roth, J. & Dai, X. 2006

    Optimization of the aerodynamic plasma actuator as an electrohydrodynamic (EHD) electrical

    device

    44th AIAA Aerospace Sciences Meeting and Exhibit, 9 - 12 January, Reno, Nevada, 2006-1203

13. Kriegseis, J.; Möller, B.; Grundmann, S. & Tropea, C. 2012

    On performance and efficiency of dielectric barrier discharge plasma actuators for flow

    control applications

    International Journal of Flow Control, 4 (3-4), 125-131

14. Kriegseis, J.; Grundmann, S. & Tropea, C. 2011

    Power consumption, discharge capacitance and light emission as measures for thrust

    production of dielectric barrier discharge plasma actuators

    J Appl Phys, 110 (1), 013305

15. Kriegseis, J.; Duchmann, A.; Tropea, C. & Grundmann, S. 2013

    On the classification of dielectric barrier discharge plasma actuators: A comprehensive

    performance evaluation study

    J Appl Phys, 114 (5), 053301

16. Hoskinson, A.; Hershkowitz & Ashpis, D. 2008

    Force measurements of single and double barrier DBD plasma actuators in quiescent air

    J Phys D Appl Phys, 41 (24), 245209

17. Ferry, J. & Rovey, J. 2010

    Thrust measurement of dielectric barrier discharge plasma actuators and power

    requirements for aerodynamic control

    5th Flow Control Conference, 28 June - 1 July, Chicago, Illinois, 2010-4982

18. Giepman, R. & Kotsonis, M. 2011

    On the mechanical efficiency of dielectric barrier discharge plasma actuators

    Appl Phys Lett, 98 (22), 221504

19. Roupassov, D. V.; Nikipelov, A. A.; Nudnova, M. M. & Starikovskii, A. Y. 2009

    Flow separation control by plasma actuator with nanosecond pulsed-periodic discharge

    AIAA J, 47 (1), 168-185

20. Little, J.; Nishihara, M.; Adamovich, I. & Samimy, M. 2010

    High-lift airfoil trailing edge separation control using a single dielectric barrier discharge

    plasma actuator

    Exp Fluids, 48 (3), 521-537

21. Opaits, D.; Shneider, M. & Miles, R. 2009

    Electrodynamic effects in nanosecond-pulse-sustained long dielectric-barrier-discharge

    plasma actuators

    Appl Phys Lett, 94 (6), 061503

22. Dawson, R. & Little, J. 2013

    Characterization of nanosecond pulse driven dielectric barrier discharge plasma actuators for

    aerodynamic flow control

    J Appl Phys, 113 (10), 103302

23. Correale, G.; Winkel, R. & Kotsonis, M. 2015

    Energy deposition characteristics of nanosecond dielectric barrier discharge plasma

    actuators: Influence of dielectric material

    J Appl Phys, 118 (8), 083301

24. Zheng, J.; Zhao, Z.; Li, J.; Cui, Y. & Khoo, B. 2014

    Numerical simulation of nanosecond pulsed dielectric barrier discharge actuator in a

    quiescent flow

    Phys Fluids, 26 (3), 036102

25. Avallone, F.; Greco, C. & Ekelschot, D. 2013

    Image resection and heat transfer measurements by IR thermography in hypersonic flows

    QIRT J, 10 (2), 188-206

26. Takashima, K.; Zuzeek, Y.; Lempert, W. & Adamovich, I. 2011

    Characterization of a surface dielectric barrier discharge plasma sustained by repetitive

    nanosecond pulses

    Plasma Sources Sci T, 20 (5), 055009

27. Starikovskiy, A.; Nikipelov, A.; Nudnova, M. & Roupassov, D. 2009

    SDBD plasma actuator with nanosecond pulse-periodic discharge

    Plasma Sources Sci T, 18 (3), 034015

28. Kotsonis, M. 2015

    Diagnostics for characterisation of plasma actuators

    Meas Sci Technol, 26 (9), 092001

29. Carlomagno, G. & Cardone, G. 2010

    Infrared thermography for convective heat transfer measurements

    Exp Fluids, 49 (6), 1187-1218

30. Schrijer, F. 2010

    Experimental investigation of re-entry aerodynamic phenomena

    PhD thesis, Delft University of Technology Publisher, Delft, The Netherlands

31. Greco, C.; Ianiro, A. & Cardone, G. 2014

    Time and phase average heat transfer in single and twin circular synthetic impinging air jets

    Int J Heat Mass Tran, 73, 776-788

32. Avallone, F.; Greco, C.; Schrijer, F. & Cardone, G. 2015

    A low-computational-cost inverse heat transfer technique for convective heat transfer

    measurements in hypersonic flows

    Exp Fluids, 56: 86, 1-12

33. Schultz, D. & Jones, T. 1973

    Heat-Transfer Measurements In Short-Duration Hypersonic Facilities

    Advisory Group For Aerospace Research And Development Paris (France), AGARD-AG-165, 1-

    149

34. Dworsky, L. N. 1980

    Modern Transmission Line Theory and Applications

    Krieger Publishing Company, Florida, USA

35. Benard, N.; Zouzou, N.; Claverie, A.; Sotton, J. & Moreau, E. 2012

    Optical visualization and electrical characterization of fast-rising pulsed dielectric barrier

    discharge for airflow control applications

    J Appl Phys, 111 (3), 033303

36. Michelis, T.; Correale, G.; Popov, I. B.; Kotsonis, M.; Ragni, D.; Hulshoff, S. J. K. & Veldhuis, L. L.

    M. 2013

Disturbance introduced into a laminar boundary layer by a NS-DBD plasma actuator

51st AIAA Aerospace Sciences Meeting including the New Horizons Forum and Aerospace

Exposition, 07 - 10 January, Grapevine (Dallas/Ft. Worth Region), Texas, 2013-0752

37. Little, J.; Takashima, K.; Nishihara, M.; Adamovich, I. & Samimy, M. 2012

Separation control with nanosecond-pulse-driven dielectric barrier discharge plasma

actuators

AIAA J, 50 (2), 350-365

38. Winkel, R.; Correale, G. & Kotsonis, M. 2014

Effect of dielectric material on thermal effect produced by ns-DBD plasma actuator

45th AIAA Plasmadynamics and Lasers Conference, 16-20 June, Atlanta, Georgia, 2014-2119

39. Roth, J.; Dai, X.; Rahel, J. & Shermann, D.

The physics and phenomenology of paraelectric One Atmosphere Uniform Glow Discharge

Plasma (OAUGDP™) actuators for aerodynamic flow control

43rd AIAA Aerospace Sciences Meeting and Exhibit - Meeting Papers, 2005, 14057-14068

40. Rios Manuel, Nudnova Maryia, Kindusheva Svetlana, Aleksahdrov Nikolay, Starikovskiy Andrey

Fast Nonequilibrium Plasma Thermalization in N2-O2 Mixtures for Different Pulse Polarities.

49th AIAA Aerospace Sciences Meeting. Orlando, Florida. Jan 2011. Paper AIAA-2011-1275

41. Popov A.N., 2011

Fast gas heating in a nitrogen-oxygen discharge plasma: I. Kinetic mechanism

J Phys D Appl Phys, 44 (28) 285201